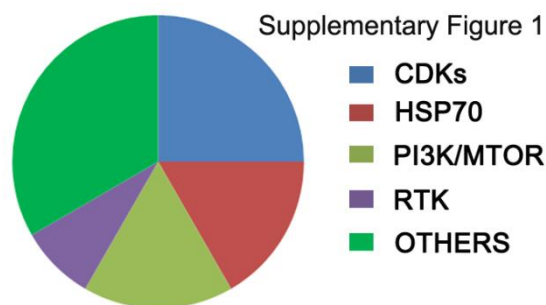
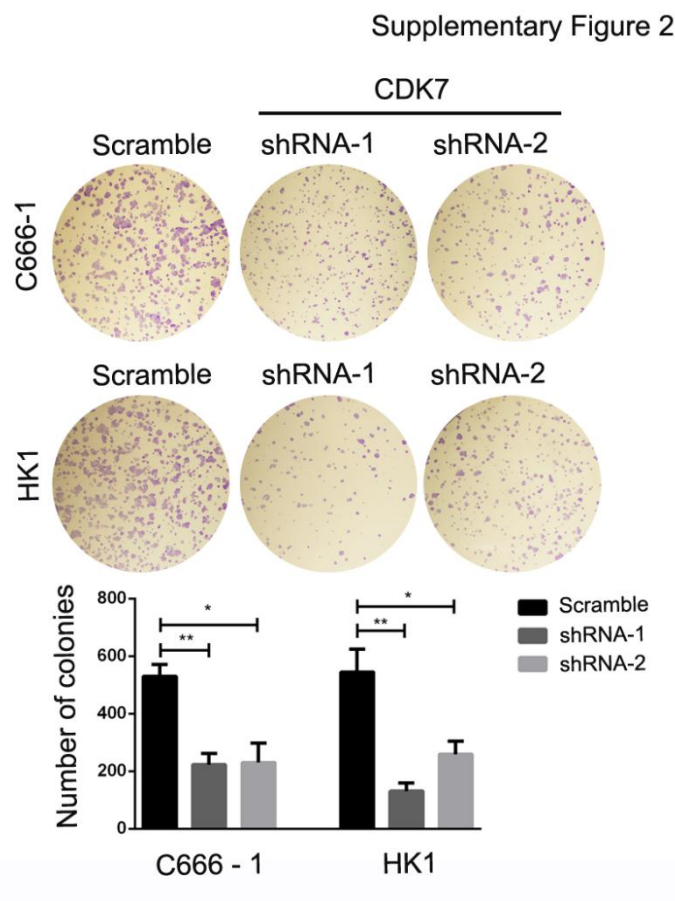


Supplementary Figures



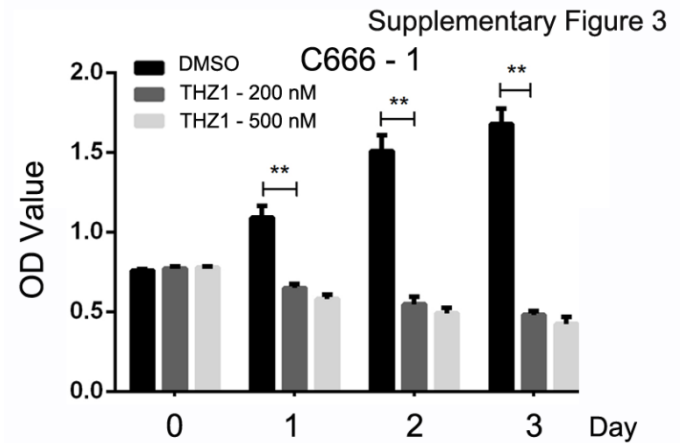
Supplementary Figure 1. Distribution of putative targets of the top-ranked small molecules



Supplementary Figure 2. CDK7 silencing significantly inhibited cells growth

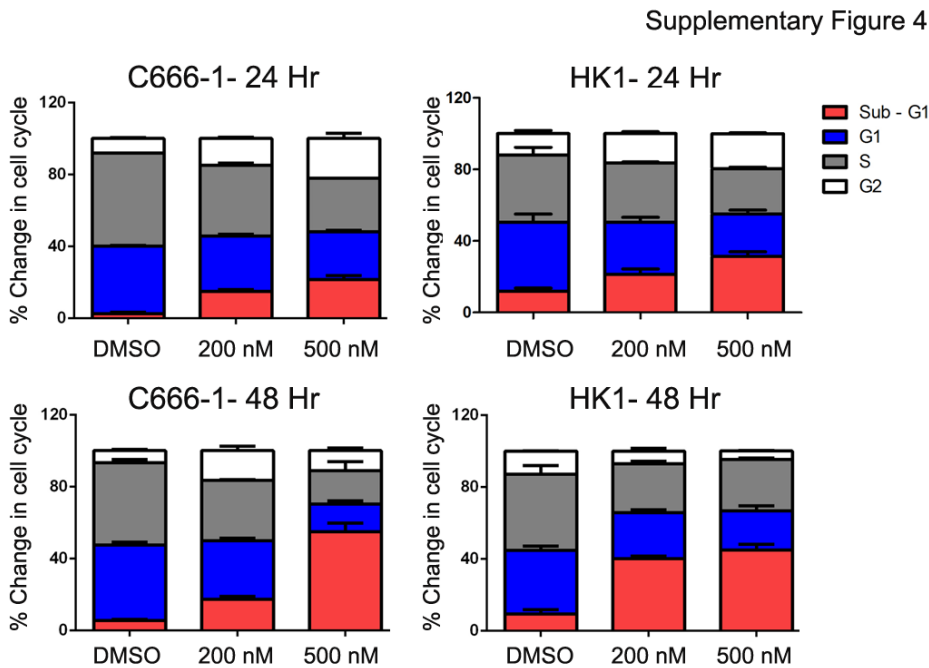
Representative images and statistical analysis of the colony formation assay in

C666-1 and HK1 cells transduced with either scramble or CDK7 shRNA virus (top figure). Results are shown as mean \pm SD of 3 independent experiments. * $P < 0.05$, ** $P < 0.01$ (bottom figure).



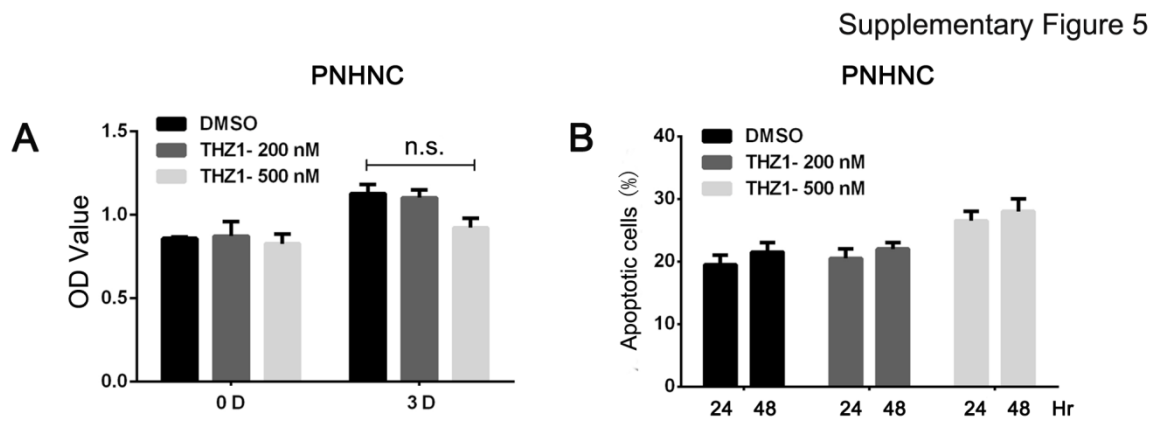
Supplementary Figure 3. Cell viability assay of C666-1 cells treated with THZ1

Cell viability assay showed the effects of THZ1 treatment in C666-1 cell lines at 1, 2 and 3 days. Bars represent mean \pm SD of 3 experiments (** $P < 0.01$).



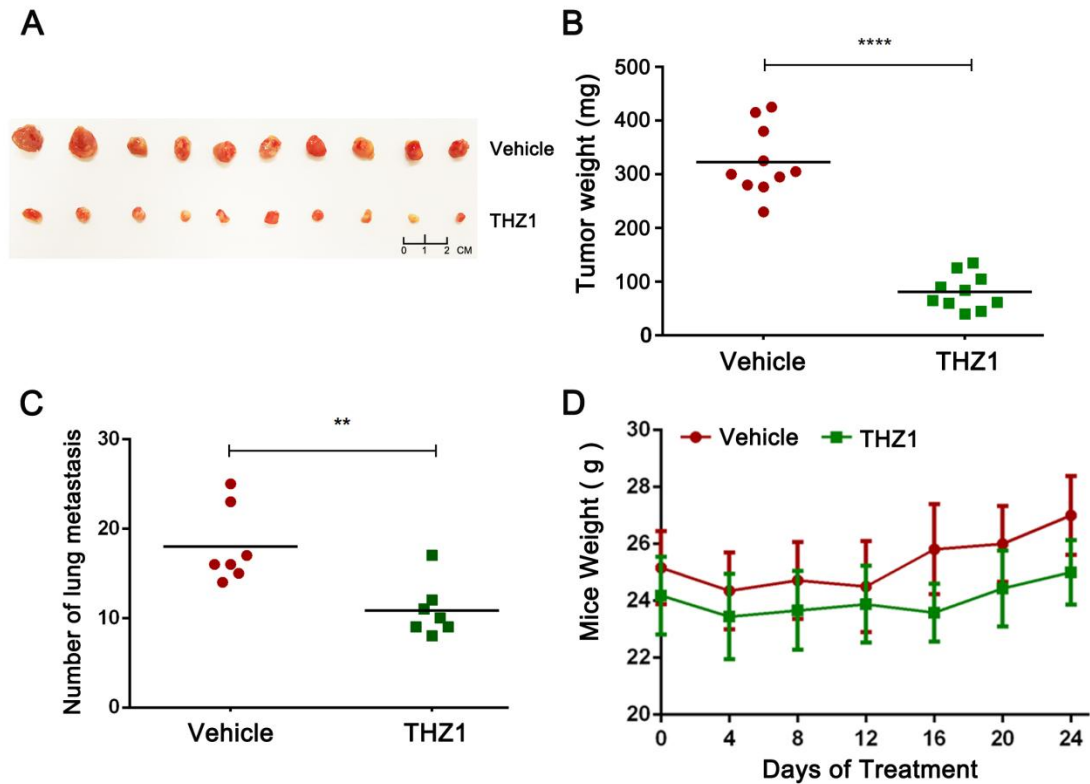
Supplementary Figure 4. Cell-cycle arrested at G2/M stage in C666-1 and HK1 cells treated with THZ1

C666-1 and HK1 cells were treated with indicated concentrations of THZ1 for either 24 or 48 hr and analyzed by flow cytometry.



Supplementary Figure 5. Cell viability (A) and apoptosis assay (B) showing the effects of THZ1 treatment in PNHNC

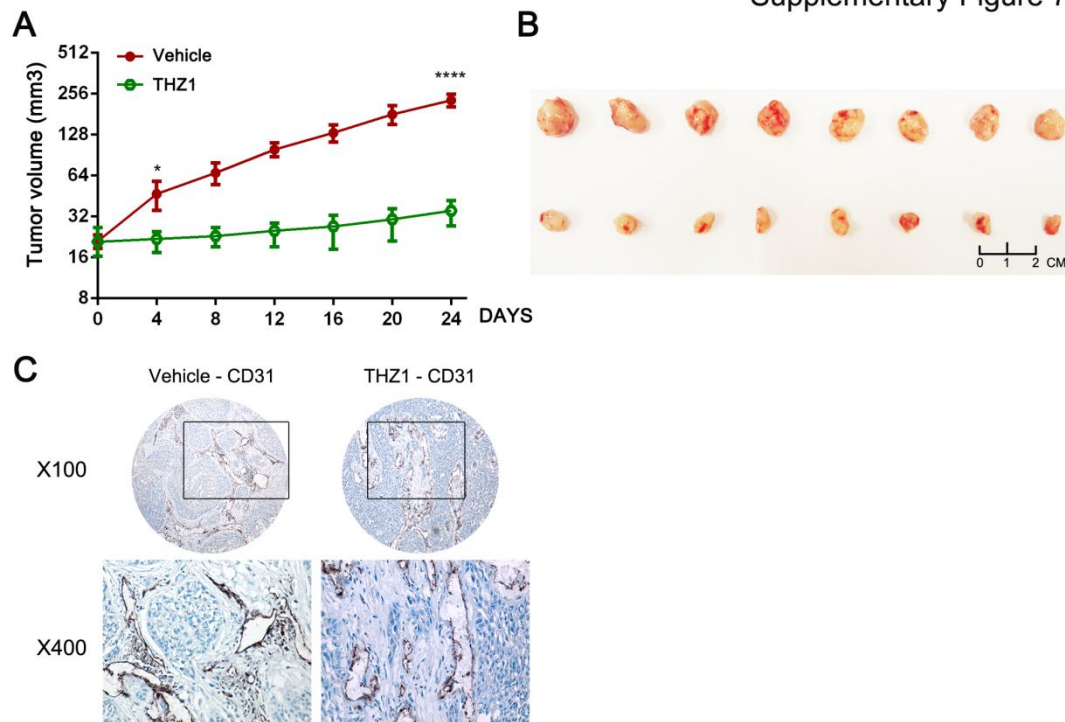
Supplementary Figure 6



Supplementary Figure 6. THZ1 potently suppressed xenografts growth and lung metastasis of NPC cells in NOD/SCID mice

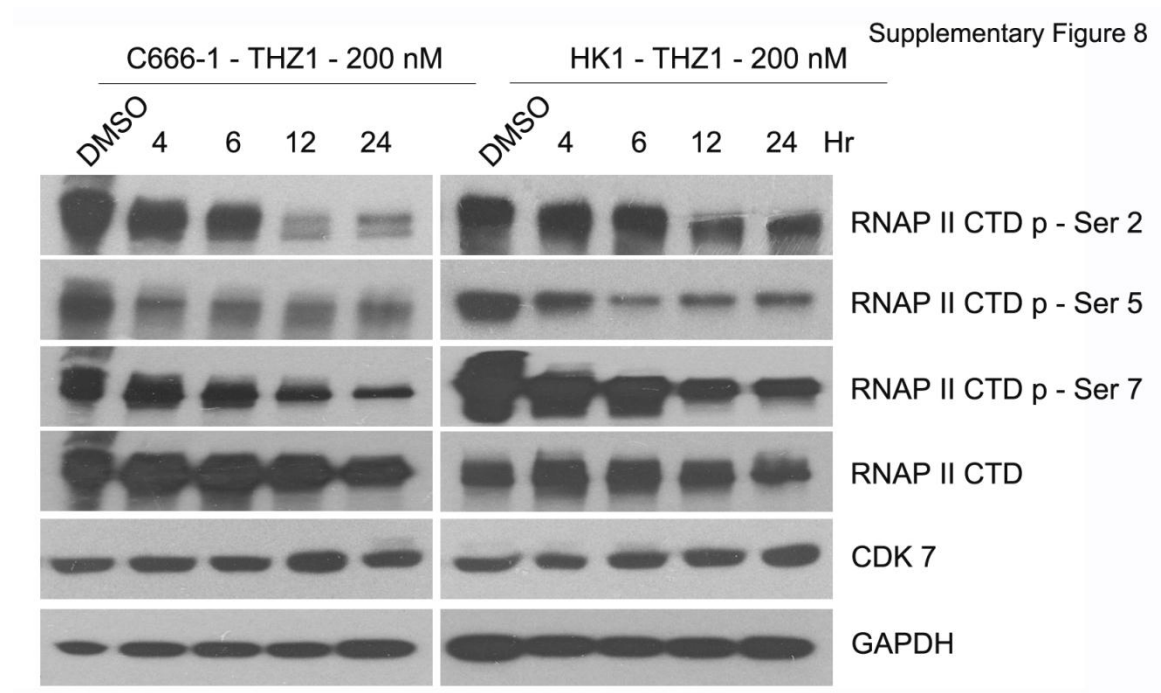
(A) Photograph of tumors from both vehicle and THZ1 (twice daily, 10 mg/kg, 24 days) treatment groups. (B) At day 24 after injection, tumors weights were measured and presented as mean \pm SD (**** P < 0.0001). (C) Visible lung metastases were counted and graphed (** P < 0.01). (D) During 24 days of THZ1 treatment, no significant loss of weight was observed in the mice.

Supplementary Figure 7



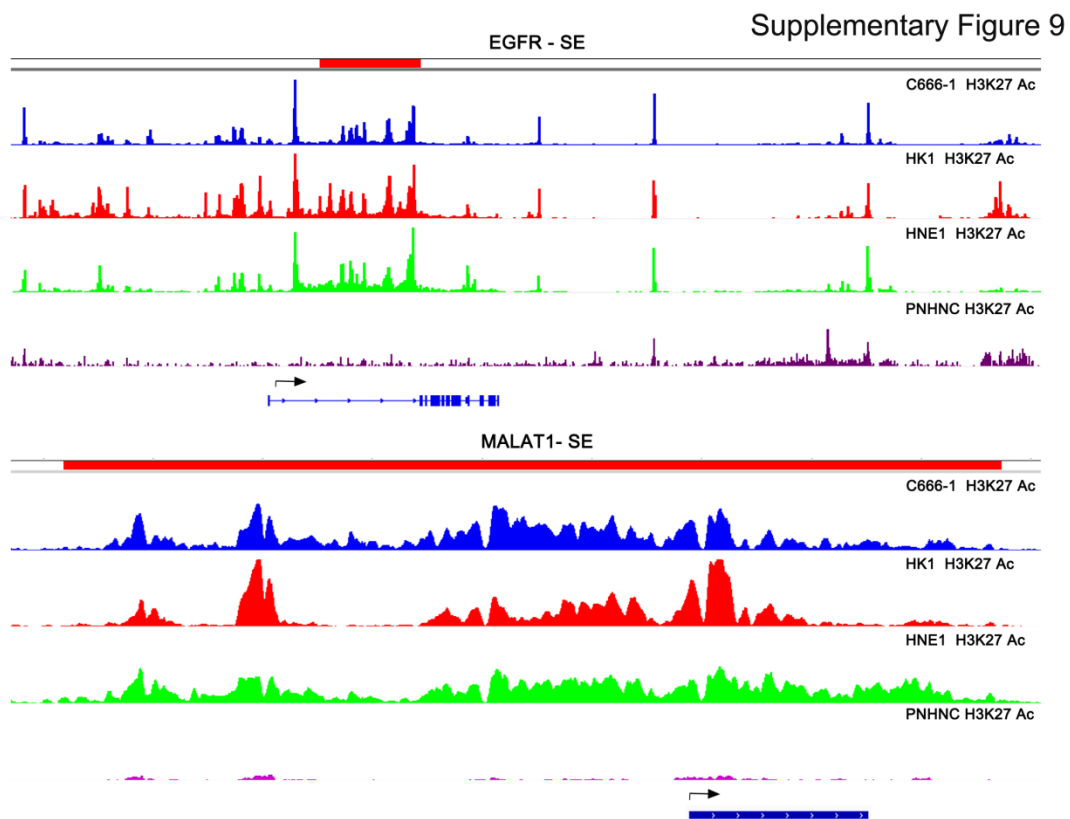
Supplementary Figure 7. THZ1 exhibited prominent anti-NPC activity in NOD/SCID mice

(A) Growth curve of xenograft treated with either THZ1 or vehicle. Data represent means \pm SD. * $P < 0.05$, **** $P < 0.0001$. (B) Photograph of tumors from both vehicle and THZ1 treated groups. (C) IHC staining of CD31 in xenograft tissue sections. Original magnification, $\times 100$ and $\times 400$.



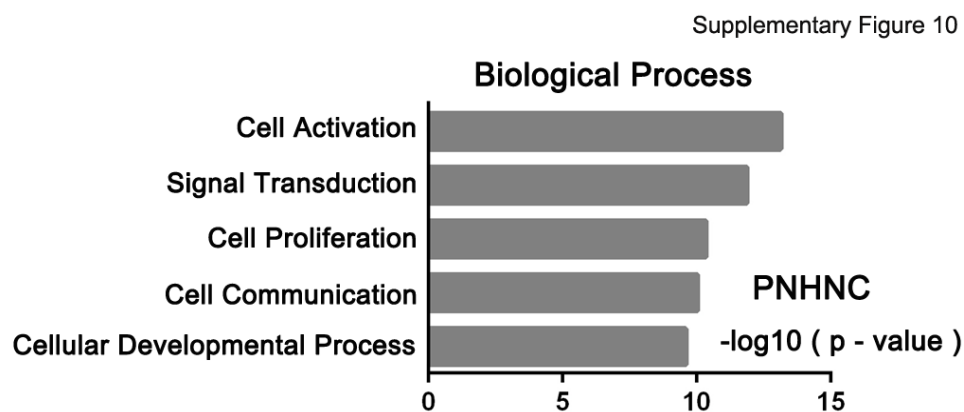
Supplementary Figure 8. THZ1 inhibited RNAPII-mediated transcription in NPC

Levels of RNA Pol II CTD phosphorylation in C666-1 and HK1 cells were decreased after treatment with either 200 nM THZ1 or DMSO at indicated time points.



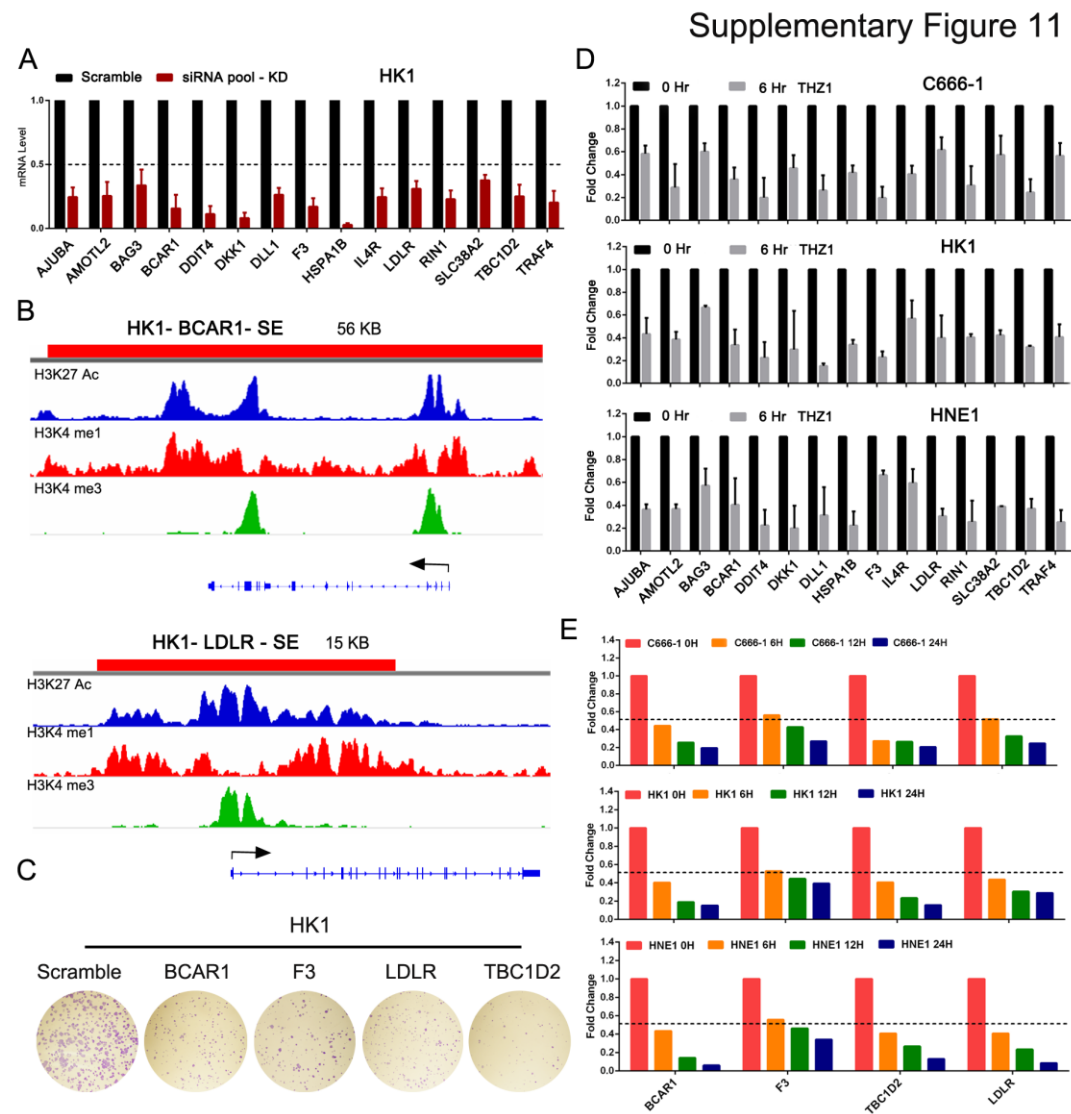
Supplementary Figure 9. Representative SE-associated genes in NPC and PNHNC

ChIP-seq profiles for H3K27ac binding at EGFR and MALAT1 gene locus in C666-1, HK1, HNE1 and PNHNC cells.



Supplementary Figure 10. Gene Ontology enrichment analysis of SE-associated

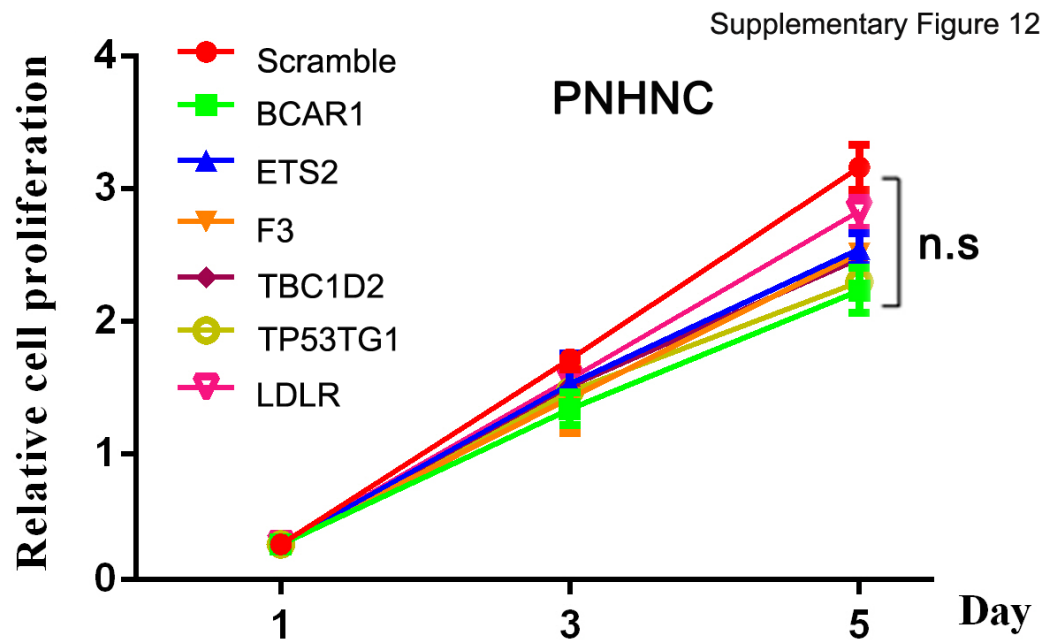
genes in PNHNC cells.



Supplementary Figure 11. Identification of novel SE-associated oncogenes in NPC

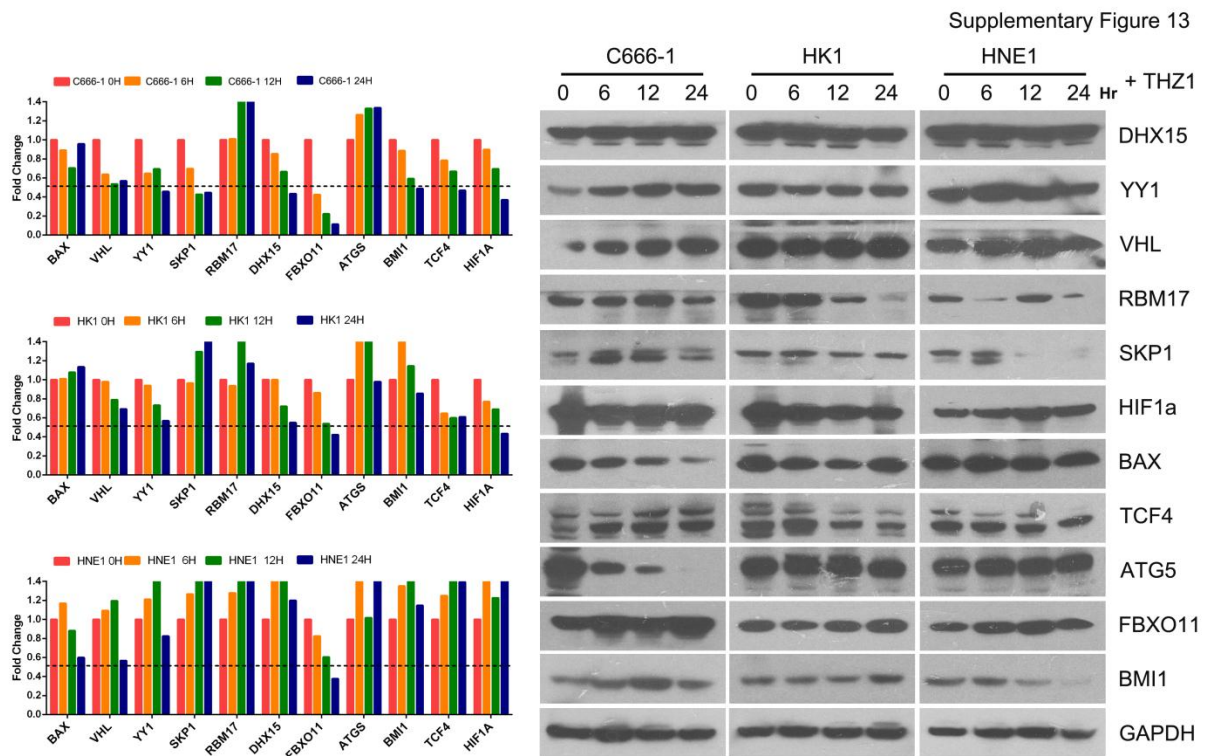
(A) Real-time PCR validation of the silencing by each siRNAs. (B) H3K27ac ChIP-seq profiles of BCAR1 and LDLR in HK1 cells. (C) Representative results of colony formation of HK1 cells transfected with indicated siRNAs. (D) Real-time PCR demonstrating sensitivity of the candidate genes to THZ1 treatment. (E) Real-time

PCR analysis showing that the RNA levels of BCAR1, F3, LDLR and TBC1D2 were rapidly decreased at indicated time points by THZ1 treatment.



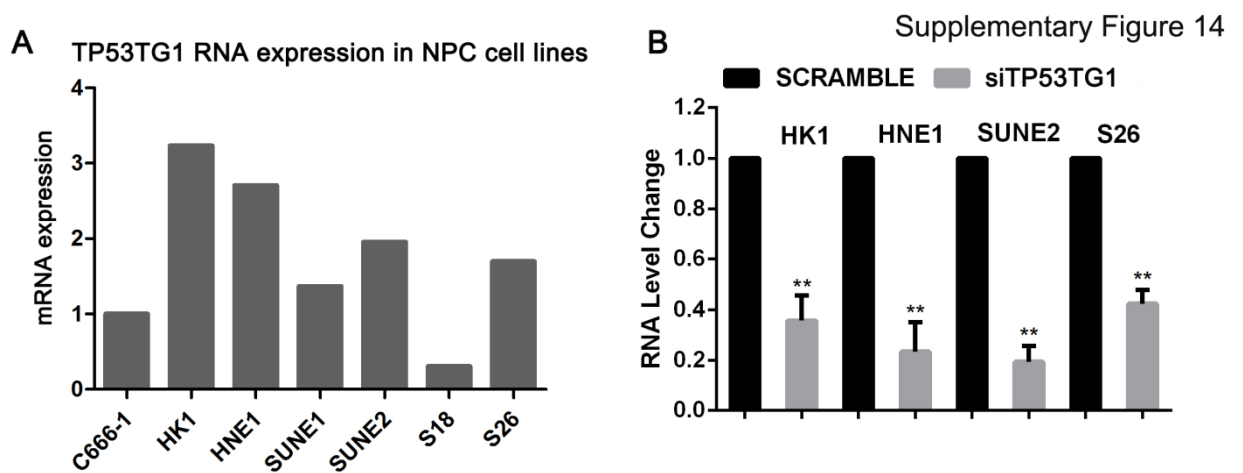
Supplementary Figure 12. Cell viability assay of PNHNC cells upon SE-associated genes knockdown

Cell viability assay showing the effects of silencing of candidate SE-associated genes in PNHNC cells, n.s. = Not significant.



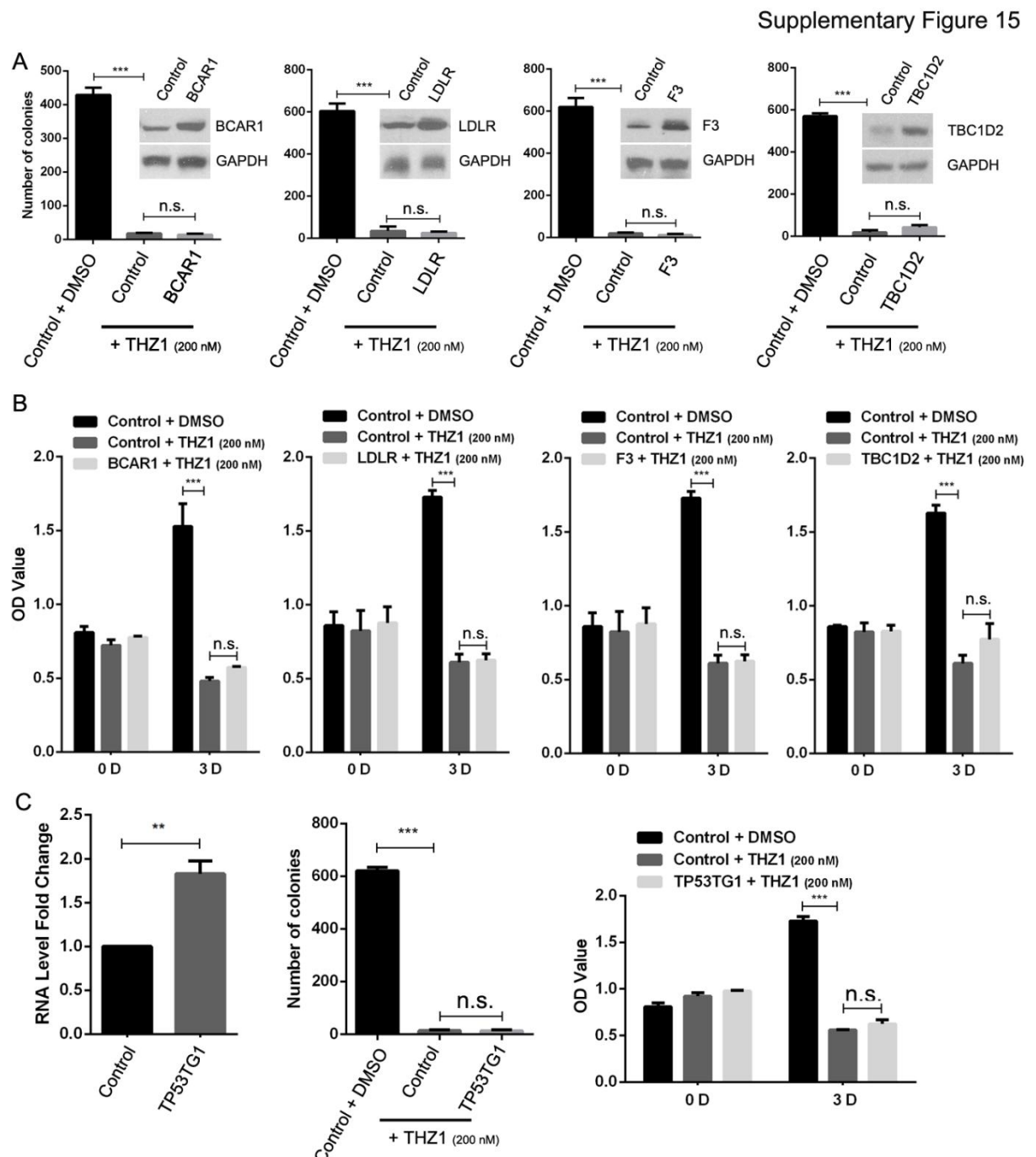
Supplementary Figure 13. TE-associated genes were less sensitive to THZ1 treatment compared with SE-associated genes

Eleven TE-associated genes were randomly selected, and fold change of their mRNA and protein levels following THZ1 treatment were quantified by real-time PCR (left) and immunoblotting assays (right).



Supplementary Figure 14. Function of a novel SE-associated LncRNA, TP53TG1, in NPC cell lines







(A) Real-time PCR analysis showing TP53TG1 RNA expression level in different NPC cell lines. (B) Real-time PCR validation of the knockdown effect of siRNA targeting TP53TG1.



Supplementary Figure 15. Over-Expression of Candidate SE-associated oncogenes cannot alleviating the cell toxicity elicited by THZ1

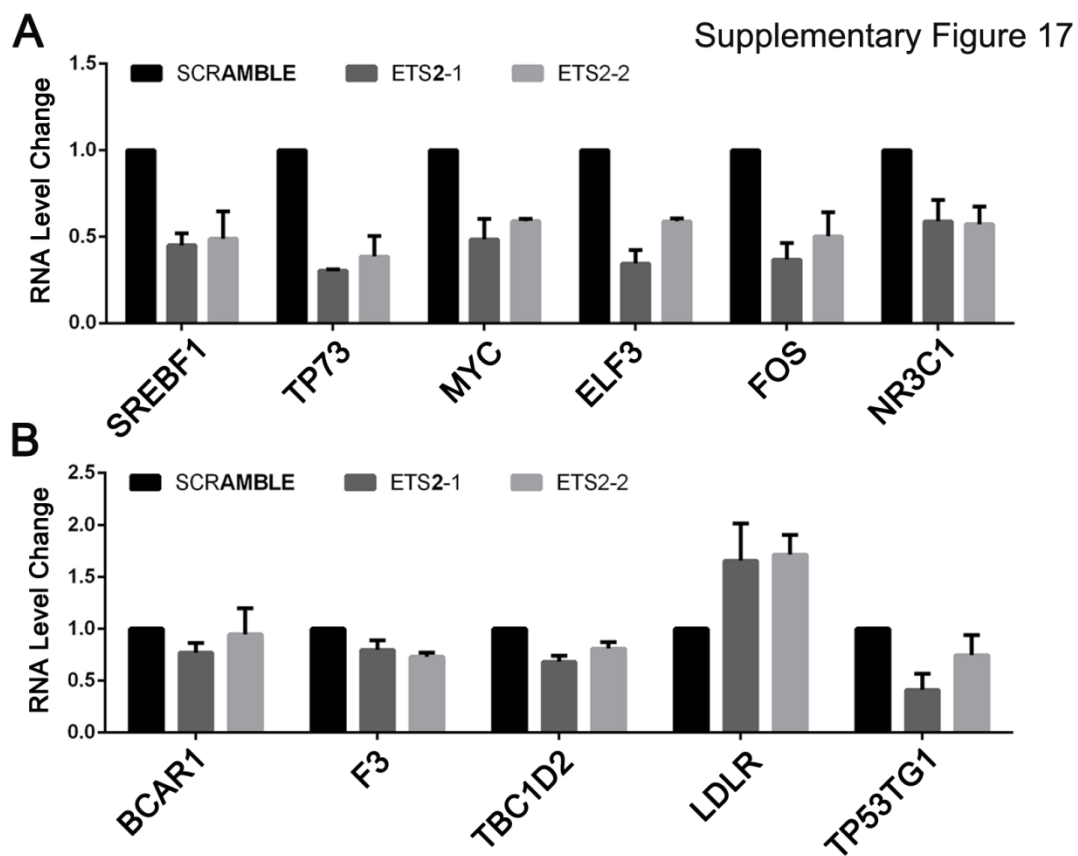
Statistical analysis of colony formation (A) and cell proliferation (B) in NPC cells treated with THZ1, in the presence or absence of over-expression of BCAR1, F3, LDLR, and TBC1D2. (C) Real-time PCR analysis of TP53TG1 over-expression (left), colony formation (middle) and cell proliferation (right) in TP53TG1 over-expressed cells treated with THZ1. Results are shown as mean \pm SD of 3 independent experiments. **P < 0.01, ***P < 0.001, n.s. = Not significant.

Supplementary Figure 16

C666-1			HNE1		
Transcription Factor	Motif	p - value	Transcription Factor	Motif	p - value
MAFK		1e-11	MAFK		1e-8
TEAD1		1e-6	TEAD1		1e-4
ETS2		1e-3	ETS2		1e-4

Supplementary Figure 16. SE-promoting master TFs in NPC

Binding motifs for MAFK, TEAD1 and ETS2, as well as their p values for the enrichment in SE constituent enhancers in C666-1 and HNE1 cells.



Supplementary Figure 17. Real-time PCR analysis showing that the RNA levels of oncogenes (A) and candidate oncogenes (B) upon ETS2 silencing.